COVER PAGE

Document downloaded by @DAEL

Sat May 9 14:57:24 2026

For personal use

When automatic English translation is provided, only the original document is authentic.
The EAA cannot be held responsible of any translation error

Bibliographical reference

Acoustoelectric Effect in Semiconductor Structures - Tool for Interface States Investigation by Complex Acoustic Spectroscopy, P. Bury, I. Bellan, I. Jamnický, J. Kúdelčík and Š. Hardoň, Acta Acustica **vol. 102** (Number 4), 2016, pp. 652-662

DOI

https://doi.org/10.3813/AAA.918982

ACTA ACUSTICA UNITED WITH ACUSTICA
Vol. 102 (2016) 652 – 662

DOI 10.3813/AAA.918982

Acoustoelectric Effect in Semiconductor Structures - Tool for Interface States Investigation by Complex Acoustic Spectroscopy

P. Bury, I. Bellan, I. Jamnický, J. Kúdelčík, Š. Hardoň
Department of Physics, Faculty of Electrical Engineering, University of Žilina, Univerzitná 1, 010 26 Žilina, Slovakia, peter.bury@fel.uniza.sk

Summary
The acoustoelectric effect resulting from the interaction between longitudinal acoustic wave and semiconductor interface has been proved to be a useful tool for the experimental study of interface states in semiconductor structures. The acoustic (acoustoelectric) deep-level transient spectroscopy (A-DLTS) technique based on the acoustoelectric effect was developed. The method uses an acoustoelectric response signal (ARS) produced by the structure interface when a longitudinal acoustic wave propagates through the structure. The bias voltage excitation pulses are then used to change the space charge distribution to measure ARS transients. Another introduced technique of acoustic spectroscopy to study interface states in MOS structures with a very thin oxide layer based on the acoustoelectric effect uses the measurement of the ARS as a function of gate voltage ($U_{ac} - U_g$ characteristics) to the determination of interface states distribution. The essential principles and theoretical background of these acoustic spectroscopy techniques that can determine the interface states parameters from the measured acoustoelectric transients and the dependence of the acoustoelectric response signal as a function of gate voltage are described. The results obtained on the representative set of MOS structures prepared on both n- and p-type Si substrates demonstrate that the introduced technique of acoustic spectroscopy can be a very useful tool for the interface states characterization.

PACS no. 43.20.YSe, 43.35.Ns

1. Introduction

Intensive investigation and consequent utilization of acoustoelectric (AE) interactions started after the observation of acoustic wave amplification by electron drift [1]. Ever since there has been a lot of experimental and theoretical works on this subject. The phenomenon of AE-interaction is extremely rich in the sense of physics of wave processes in solids that deals with the excitation and propagation of acoustic waves of high frequency (usually 1 – 1000 MHz) and their interaction with electrons in solids. However, a large number of papers deal with intermediate AE-interaction; with different types of nonlinearity arising with the increase of sound intensity; with the role of traps, surface states, and other factors describing semiconductors; with the influence of illumination, magnetic field, etc. [2, 3, 4, 5].

Recently, the AE effect in semiconductor structures has been shown to be an effective tool for the characterization of electrical properties and experimental study of semiconductors and semiconductor structures. The AE interactions were utilized to surface and interface state determination, carrier transport properties characterization including conductivity and carrier mobility measurement, the interface state determination, $2D$ and $1D$ electron or hole system investigation, hf AE effect in electron tunneling devices and number of important devices utilization [6, 7, 8, 9, 10, 11, 12, 13].

Semiconductors are the fundamental materials of the electronic industry because their properties can be manipulated over wide ranges through the control of impurities and other imperfections. While shallow impurities generally contribute extra charge carriers, electrons or holes and introduce minor perturbations in the crystal other impurities and a variety of lattice defects (vacancies, antisite defects, self-interstitials, etc.) constitute a more severe local perturbation, give rise to bound states that are considerably more localized, and often have energies deep in the band gap. We know all such impurities, lattice defects, and impurity-defect complexes as deep centers that act primarily as carrier traps or recombination centers.

During the recent past, the semiconductor interfaces in a metal-semiconductor contacts, semiconductor-insulator interfaces and semiconductor heterostructures are most important concepts in semiconductor devices and circuits that play a revolutionary role in microelectronics. New

Received 26 February 2016,
accepted 10 May 2016.

© S. Hirzel Verlag · EAA

Document downloaded by @DAEL, 2026-05-09 14:57:29 - personal use only

technologies, however require smaller devices, sharper transitions and higher number of preparation steps. Narrower transitions require sharper doping profiles and subsequently lower temperatures during the preparation processes. These processes introduce defects at the interfaces (interface states) that hardly can be removed by thermal treatment and represent another new group of fabrication-induced defects. To this group belong also interface states at semiconductor-insulator heterojunction in MOS (metal-oxide-semiconductor) structures that play an important role in determining their electrical characteristics that are important for practical use in semiconductor devices. A silicon-silicon dioxide (Si/SiO_2) structure mostly prepared by thermal oxidation at above $800\,^oC$ in oxidizing atmospheres is widely used for MOS devices [14]. Because the high temperature oxidation results in high interfacial stress producing the interface defect states [15], the low temperature direct oxidation methods such as plasma oxidation, metal-promoted oxidation or method of nitric acid oxidation of Si (NAOS) were developed [16, 17, 18, 19]. Producing a very thin oxide layer, metal oxides with high dielectric permittivity (high κ dielectrics) can find a successful application as a replacement for SiO_2 gate insulator to break through its physical limit [20, 21]. Although due to the many improvements in preparation technology, the density of interface states, especially at SiO_2/Si interfaces is usually very low, still it can seriously affect electrical properties of MOS devices and the interface states need to be well characterized.

The interface (deep) states of semiconductor structures have been extensively studied and many useful experimental methods have been developed to characterize them [22, 23, 24, 25, 26, 27]. Following the work of Lang [28], deep-level transient spectroscopy (DLTS) has become most powerful technique commonly used for the characterization of semiconductors and semiconductor structures because it reveals information about several characteristics (activation energy, capture cross-section, concentration) of electrically or optically active defects present in such materials. Several useful variants of DLTS have been developed [29, 30, 31, 32] and many attempts to improve the defect resolution capabilities of DLTS introducing different types of transient analysis procedure have been reported [33, 34, 35, 36, 37].

Several methods were developed also for the interface states distribution determination. The simplest and very often used technique utilizes $C-V$ measurements at very low frequencies [15]. However, a high leakage current in the case of a very thin oxide layer disturbs $C-V$ measurements. Later, computational methods to fit high frequency $C-V$ characteristics especially for MOS capacitors with high-κ dielectrics have been presented [38, 39]. To find the distribution of interface states, the DLTS can be also used [40]. Recently, the X-ray photoelectron spectroscopy (XPS) under bias was used to obtain the energy distribution of interface states at very thin oxide/Si interfaces determination [41]. Some attempts to determine the interface states density using the acoustoelectric effect resulting from the interaction of surface acoustic wave (SAW) with interfaces were also performed [42].

When the acoustoelectric effect (AE) in semiconductor structures has been shown to be an effective tool for the characterization of electrical properties and experimental study of semiconductors, two basic modifications of acoustoelectric (acoustic) deep-level transient spectroscopy (A-DLTS) were independently introduced. The former SAW technique uses a nonlinear AE interaction between the SAW electric field and free carriers in an interface region which generates a transverse acoustoelectric signal (TAS) across the structure. Transient measurements of the rise or fall times of the resulting dc part of the TAS [43, 44, 45] and as well as the development of the hf part of TAS after injection pulse, have been used to study interface traps [46, 47]. The latter longitudinal acoustic wave (LAW) technique uses an acoustoelectric response signal (ARS) observed at the interface of the semiconductor structure when a longitudinal acoustic wave propagates through the structure [48, 49]. Because the ARS is very sensitive to any changes in the space charge distribution in the interface region its time development after an injection pulse has been applied to the structure was utilized to develop the acoustic version of deep-level transient spectroscopy (A-DLTS) [49, 50] and later its dependence on external voltage ($U_{ac} - U_g$ curves) enabled to develope the new technique of acoustic spectroscopy [51, 52]. Both techniques were then used to study the interface states properties including their activation energy, cross-section, concentration and interface states distribution. The A-DLTS technique was on the continual upgrade in both experimental arrangement and the way of A-DLTS spectra evaluation, that is from the acoustic version of Lang‘s DLTS [53] originally developed for capacitance measurements [28], through the computer evaluation of isothermal ARS transients [49] up to the present FFT (Fast Fourier Transformation) analysis of ARS transients and LABVIEW system for the experiment operation.

In the present contribution, the main theoretical and experimental principles of two basic techniques of acoustic spectroscopy in their last versions as a complex tool for the investigation of interface states in MOS structures using the ARS produced by the pressure modulation of LAW are presented. The results obtained using these techniques on the set of MOS samples with oxide layers of different thickness prepared on different type of semiconductor are presented, compared and discussed.

2. Theoretical principles

The interface states at MOS interfaces change their charge state depending on whether they are filled or empty and can be of two categories, donor type (neutral when filled and positive when empty) and acceptor type (negative when filled and neutral when empty). However, the state occupancy varies with gate voltage U_g that changes the

Document downloaded by @DAEL, 2026-05-09 14:57:29 - personal use only

band bending ($q\phi_s$). The gate voltage U_g relates to surface potential ϕ_s following the equation [15]:

$$U_g = \phi_s - \frac{Q_s(\phi_s)}{C_{ox}} - \frac{Q_{it}(\phi_s)}{C_{ox}} + \phi_{ms} - \frac{Q_{ox}}{C_{ox}}, \quad (1)$$

where Q_s is the semiconductor charge, ϕ_{ms} is work function difference between gate and semiconductor, Q_{it} is trapped charge at the interface state, Q_{ox} is oxide charge and C_{ox} is oxide capacitance. The last two terms in the Eq. (1) represent the flat band voltage U_{fb}. The charge trapped into interface states changes with any change in the band bending.

The basic principle of an acoustoelectric response signal creation can be explained using the idea of an acoustic wave passing through the MOS structure characterized by the particular space charge region at the interface. Schematic illustration of such MOS structure with interface is shown in Figure 1. Here the buffer rod is used to separate out the acoustoelectric signal produced by MOS structure from the input acoustic pulse and the capacitor C_v protects the receiver input against the *dc* voltage. The *ac* voltage U_{ac} represents the acoustoelectric signal created by the MOS interface due to the interaction with an acoustic wave. The acoustic wave characterized by acoustic pressure $p = p_0 \cos(\omega t - kx)$, following the pressure modulation of charge density at the MOS interface region evokes the potential difference that manifests as an ARS signal. The ARS produced by the MOS structure propagating by longitudinal acoustic wave can be then expressed using the similarity with the case of electromechanical capacitance transducer of thin planar structure ($d \ll \lambda$) for which the ARS, $U_{ac} \sim U(\delta C/C)$, coincidently provides the relative capacity change relation [48]

$$\frac{\delta C}{C} = \frac{\delta x}{x} = \frac{\delta \sigma}{K} = \frac{p}{K}, \quad (2)$$

where $\delta x/x$ is the relative deformation of the capacitor in the x-axis direction, p_0 is the acoustic pressure amplitude, σ is the mechanical stress produced by the acoustic wave and K is the elastic modulus.

Using Equation (1) and regular capacitance representation of MOS structure [15], the ARS produced by the MOS structure can be expressed by

$$U_{ac} = \phi_s \frac{p}{K_s} - \frac{Q_s(\phi_s)}{C_{ox}} \frac{p}{K_i} - \frac{Q_{it}(\phi_s)}{C_{ox}} \frac{p}{K_i} \quad (3)$$

with the amplitude

$$U_{ac}^0 = \left| \phi_s \frac{p_0}{K_s} - \frac{1}{C_{ox}} \frac{p_0}{K_i} \left[Q_s(\phi_s) + Q_{it}(\phi_s) \right] \right|, \quad (4)$$

where K_s and K_i are the elastic moduli of the semiconductor and insulator, respectively, and the physical meaning of the absolute value is that the ARS cannot differ the polarity of total charge or potential. For the oxide charges, we can suppose their influence only in rare cases and in the following considerations, they are neglected.

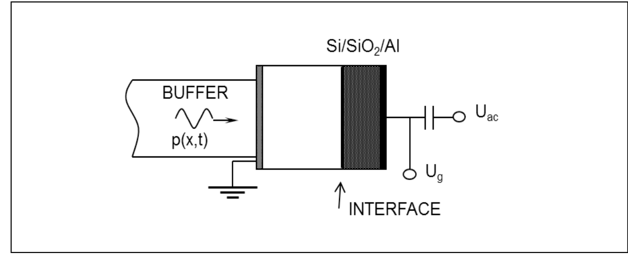

Figure 1. Schematic illustration of MOS structure passing by the longitudinal acoustic wave.

The theoretical principle of A-DLTS technique [49, 50, 54] is based on the fact that the change of the amplitude of the measured ARS, δU_{ac}^0 after an injection pulse has been applied to the structure is proportional to the nonequilibrium charge at the interface and the decay time constant associated with the relaxation of the ARS amplitude is then a direct measure of the time constant associated with the relaxation processes of injected carriers. Therefore, the ARS amplitude time dependence can be written as

$$U_{ac}^0(t) = U_0 + U_1 \exp\left(-t/\tau \right), \quad (5)$$

where U_0 is the original ARS due to the acoustoelectric interaction of acoustic wave and charge at the interface of MOS structure and U_1 represents the increase of the ARS due to the injection pulse. The time constant characterizing the relaxation processes after applied injection pulse can be expressed for electrons by

$$\tau^{-1} = \gamma_n \sigma_n T^2 \exp\left(-\frac{E_t}{k_B T} \right), \quad (6)$$

where σ_n is the electron capture cross section, γ_n is constant, E_t is the interface state activation energy related to the bottom of conduction band, k_B is the Boltzmann's constant and T is the thermodynamic temperature. The analysis of the time dependence of the ARS at different temperatures then allows to construct the A-DLTS spectra and following to determine the activation energy of interference states E_t and corresponding cross section σ_n. The acoustoelectric investigation of the MOS structure [14] validate that the ARS follows the accumulated charge behavior over the capacitance one.

The theoretical principles of the determination if interface state distribution from the $U_{ac}^0 - U_g$ characteristics come from the following analysis of the ARS given by Eqs. (3) and (4). If the situation in the structure without any interface states ($Q_{it} = 0$) is indexed as "ideal" and then, using Eqs. (1) and (4) can be expressed after particular formal modifications in the form

$$U_{ac}^0(\text{ideal}) = \left| \frac{p_0}{K_s} \left| U_g - U_{fb} \right| + \frac{Q_s}{C_{ox}} \frac{K_i - K_s}{K_s K_i} p_0 \right|. \quad (7)$$

As it can be seen from Equation (7), the ARS of ideal MOS structure is the superposition of a linear term with zero at flatband voltage and a term representing the contribution from the semiconductor charge Q_s. To determine

Document downloaded by @DAEL, 2026-05-09 14:57:29 - personal use only

the energy distribution of interface states, it is necessary to know the dependence of the semiconductor charge on the surface potential for an ideal MOS structure. This dependence can be obtained using the Terman's model [15].

The quantity Q_{it} depends on the interface charge state and its occupation by carriers and can be generally expressed as [39]

$$Q_{it} = q \int_{E_v}^{E_i} D_{it}(E_t) \left[1 - f(E_t)\right] \mathrm{d}E_t - q \int_{E_i}^{E_c} D_{it}(E_t)\, f(E_t)\, \mathrm{d}E_t, \quad (8)$$

where q is the elementary charge, D_{it} is the density of the interface states, E_v and E_c are the energies of the valence and conduction band edges, E_i is the intrinsic Fermi level and $f(E_t)$ is the occupation probability of the energy level E_t.

The interface trapped charge can be expressed through the deviation of the ARSs of real and ideal structures, comparing Equations (4) and (7), as

$$Q_{it} = S\left(U_{ac}^0 - U_{ac}^0(\text{ideal})\right), \quad (9)$$

where $S = C_{ox} K_s / p_o$. The interface state density D_{it} can be then expressed, describing the $U_{ac}^0 - U_g$ curves for ideal and real MOS structures, by the relation

$$D_{it}(E_t) = \frac{1}{q}\left|\frac{\mathrm{d}Q_{it}}{\mathrm{d}\phi_s}\right| = \frac{1}{q}\left|S\frac{\mathrm{d}(U_{ac}^0 - U_{ac}^0(\text{ideal}))}{\mathrm{d}\phi_s}\right|. \quad (10)$$

Equation (10) allows then to determine the distribution of interface states from the measured ARS.

The energy level E_t in the band gap of the semiconductor, corresponding to interface traps density $D_{it}(E_t)$, can be calculated then from the equation [15]

$$E_t = E_v + \frac{E_g}{2} + q\,\phi_s \pm k_B T \ln\left(\frac{N_{D,A}}{n_i}\right), \quad (11)$$

where E_g is the semiconductor band gap energy, $N_{D,A}$ is the concentration of the donors or acceptors and n_i is the intrinsic concentration. The plus sign in Eq. (11) corresponds to the n-MOS and the minus sign corresponds to the p-MOS structure.

In the case of real MOS structure with the interface states, the $U_{ac}^0 - U_g$ characteristics contain information about the charge at the interface states and because the ARS reflects directly changes in the space charge distribution at the interface region, the interface state density can be extracted comparing the real (measured) and ideal (calculated) $U_{ac}^0 - U_g$ curves (Eq. (10)). As the interface state occupancy varies with the gate bias, the corresponding changes manifest as hops on the real $U_{ac}^0 - U_g$ curve comparing with the ideal one [52].

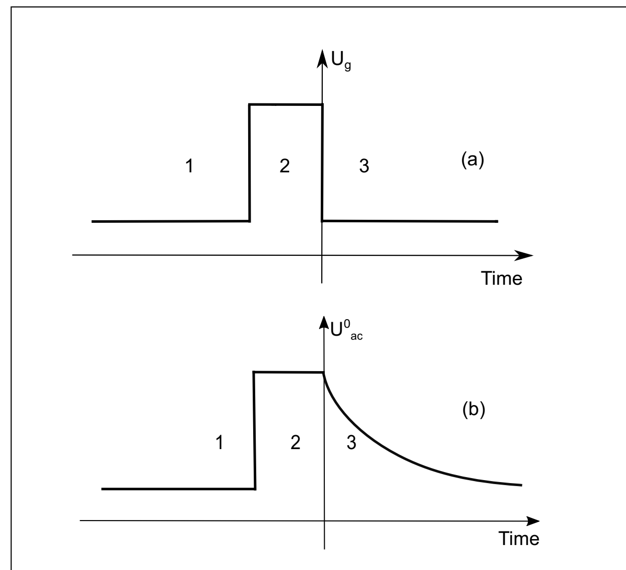

Figure 2. Sequence of applied gate voltage pulse (a) and resulting acoustoelectric transient (b).

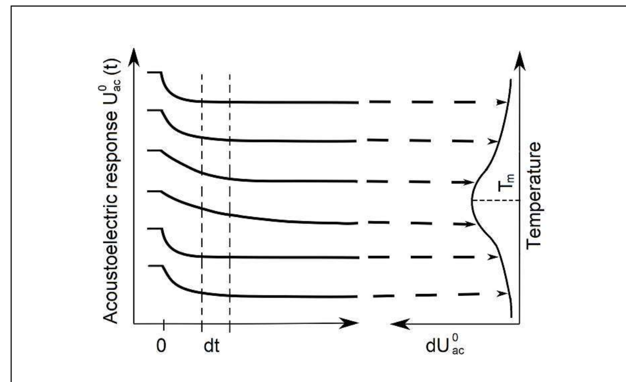

Figure 3. Schematic illustration of acoustoelectric transients analysis.

3. Experimental principles

3.1. Acoustic deep level transient spectroscopy (A-DLTS)

The present measurement technique of A-DLTS is based on the computer-evaluated transients measured at fixed temperatures. The differential ARS, δU_{ac}^0 is then monitored as a function of temperature and peaks with maxima at the temperature for which the emission rate is the same as the adjusted sample rate window represent A-DLTS spectra [50, 53, 54].

The principle of our A-DLTS measurements consists then in the special analysis of the acoustoelectric transient signal after an injection pulse (Figure 2) using a set of emission rate windows similarly as in the case of the DLTS technique developed for the capacitance transients. Relaxation times of an exponential transient signal are displayed using selected rate windows (Figure 3) and a response peak occurs at the temperature where the trap emission rate is within the window. The emission rate windows

Document downloaded by @DAEL, 2026-05-09 14:57:29 - personal use only

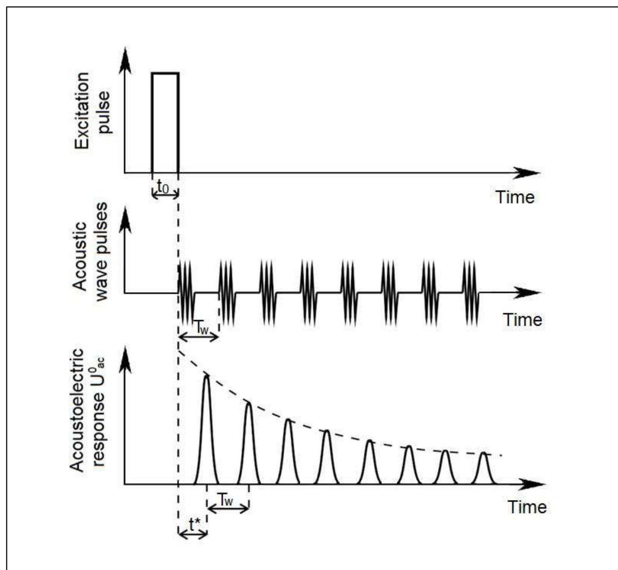

Figure 4. Schematic illustration of the time arrangement of some experimental parameters, t_0 is the bias voltage pulse width, $f_w = 1/T_w$ is the rate frequency and t^* is the transverse time through the buffer rod.

are precisely determined by setting of time interval δt after the bias injection pulse and the differential acoustoelectric response signals δU^0_{ac} can be monitored as a function of temperature. The peaks with the maxima at the temperature for which the emission rate is the same as the adjusted window are then the result of the measurement.

The software for the calculation allows to use the acoustic version of Lang's original scheme [53] or the correlation procedure with higher on/line filters and rectangular weighting function [50] or FTT analysis that can describe more effectively dynamic processes and by that also acoustoelectric responses. In the case of very close interface state levels the deconvolution technique can be used, too. The technique allows then a single transient to be sampled at many different sample rates permitting several decades of time constants to be observed in one thermal scan without permanent processing redundant data. The schematic illustration of the time arrangement of some experimental parameters corresponding to the isothermal transients scanning process is given in Figure 4.

Using the well known relation expressing the temperature dependence of the relaxation time characterizing the acoustoelectric transient (Eq. (6)) the activation energy, E_t, and corresponding capture cross-section, σ_n, can be determined. The Arrhenius plot can be then constructed using the relation

$$\left[\ln\left(\tau^2 T_m^2\right) \sim E_t\left(1/T_m\right)\right]. \tag{12}$$

3.2. Density of interface states determination

To understand the basic principles of the density of interface states determination from the $U^0_{ac} - U_g$ characteristics, the simulated ideal and real $U^0_{ac} - U_g$ characteristics of the n-type MOS capacitor (Figure 5) are compared with the

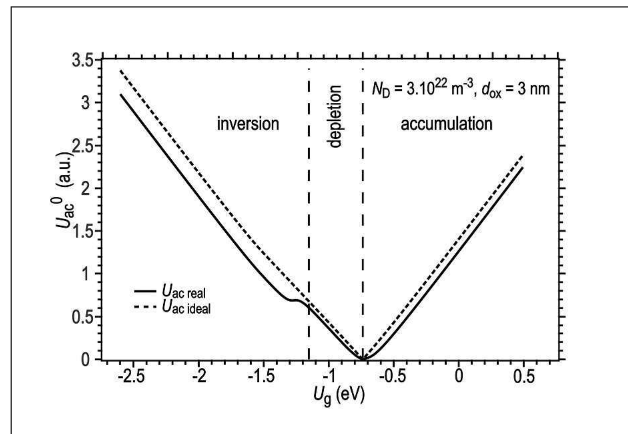

Figure 5. Theoretical $U^0_{ac} - U_g$ characteristic of "ideal" n-MOS structure-without any interface states (dotted line) compared with simulated "real" $U^0_{ac} - U_g$ curve corresponding to two kinds of interface states (solid line).

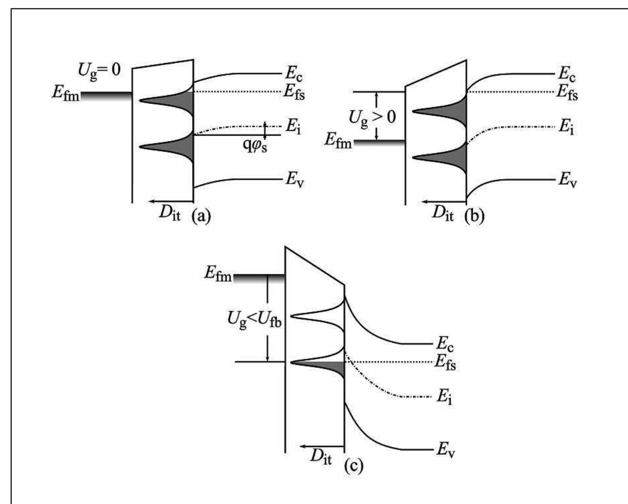

Figure 6. Energy band diagrams of n-type Si based MOS structure with no bias (a) and as a function of bias at accumulation (b), and at inversion (c) representing the interface states empting and/or occupying processes of two kinds of interface states. Energy values E_{fs} and E_{fm} are the Fermi levels in the silicon and in the metal, respectively.

changes in the bands bending of such structure containing assumed two kinds of donor type interface states (Figure 6).

At zero bias, the surface potential ϕ_s causes the weak accumulation when and the semiconductor bands bend as shown in Figure 6a. The interface states present above silicon Fermi level E_{fs} are empty while those below E_{fs} are occupied by electrons. By the application of a positive bias U_g (continuously accumulated), the additional electrons are attracted to the silicon surface and zero voltage bands bending increases and at very large positive bias, the electron density at the semiconductor surface exceeds electron density in the bulk. The increase of positive gate voltage results in the increase of accumulation charge and consequently the increase of the ARS.

Document downloaded by @DAEL, 2026-05-09 14:57:29 - personal use only

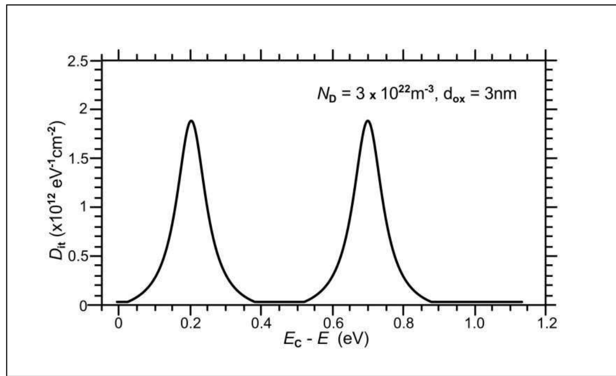

Figure 7. Simulated distribution of interface states calculated using the ideal and simulated real $U_{ac}^0 - U_g$ curves from Figure 5.

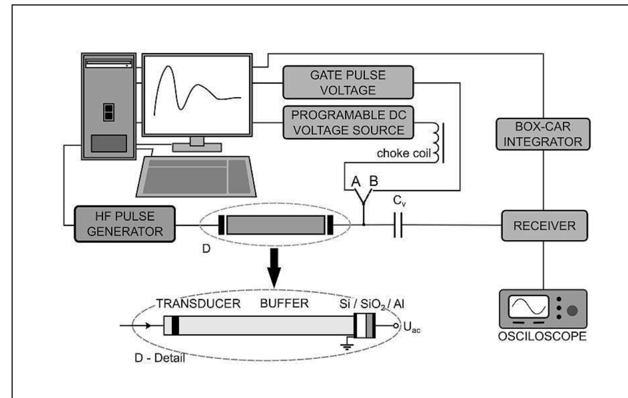

Figure 8. Block diagram of the experimental setup with the detailed sample configurations (D-detail) for A-DLTS measurement (B) and measurement of $U_{ac}^0 - U_g$ characteristics (A).

In the case of interface states present close to the conduction band, the change in band bending at positive bias leads to the filling of interface states initially present above Fermi level (Figure 6b). That causes a decrease of electron density at the semiconductor surface as well as interface state charge Q_{it} that results in the decrease of the ARS as far as all states are filled.

Applying a negative bias, at the first electrons are eliminated from the semiconductor surface until flatband occurs ($U_{ac} = 0$) and continuing from the flatband electrons are repelled from the semiconductor surface resulting in the formation of a depletion region. As negative gate bias is increased, the depletion region widens following the formation of inversion layer where the surface hole density increases. Simultaneously, the interface states present initially below Fermi level become unoccupied (Figure 6c), which results in the decrease of Q_{it} and consequently the measured ARS. The presence of another interface states causes another drop of the ARS. Calculating the difference between the ideal and simulated real $U_{ac}^0 - U_g$ curves and using the Eq. (10), the simulated interface states distribution was determined as shown in Figure 7.

However, the tunneling current for the very thin oxide layer ($<$ 10 nm) influences the division of the applied voltage Ug between the semiconductor and insulator layer and for the oxide layer thickness $<$ 2 nm, the whole applied voltage practically spreads across the semiconductor, especially in the range of inversion [56]. Concerning the tunneling process, the transport of free charge curriers through the thin oxide layer caused by applied electric field has to be taken into account in cases where the tunneling current following with the Fowler-Nordheim mechanism [57] induces additional change of the ARS

$$\Delta U_{ac} = A \left(U_g^2 + B \right) \exp\left(-\frac{C}{U_g} \right), \qquad (13)$$

where A, B and C are constants. The simulation of the "ideal" ARS inclusive the calculation of tunnel current contribution gives a new ideal ARS, U_{ac}^0(tunnel).

Except the leakage current, the Schottky contact on the metal-semiconductor interface can be also the reason for some deviation in the measured $U_{ac}^0 - U_g$ dependence, especially near the flatband. To eliminate this influence, the added capacitance of Schottky contact [23].

The sensitivity of presented method depends on the accuracy of the acoustoelectric response signal U_{ac}^0 measurement, the acoustic signal stability and the ability to distinguish the changes ΔU_{ac} between the real and "ideal" $U_{ac}^0 - U_g$ characteristics.

4. Experimental details

The experimental arrangement of the measurement technique for both measurement of A-DLTS spectra and measurement of characteristics is shown in block diagram in Figure 8. The A-B key symbolically represents the different arrangement in the case of these individual techniques. The computer using the LABVIEW system was used to trigger the apparatus - Pulse Modulator and Receiver (MATEC 7700), to drive bias voltage as well as to record and evaluate isothermal transients in the case of the A-DLTS and register the ARS as a function of applied bias voltage ($U_{ac}^0 - U_g$ characteristics). A longitudinal acoustic wave of frequency 13.2 MHz was generated using $LiNbO_3$ transducer in the arrangement illustrated in the D-detail. The ARS produced by the MOS structure was then detected by Receiver, selected using the Gated Integrator and Box-car Averager (SRS), recorded and stored by a computer. The quiescent bias voltage pulses of $100 - 200$ ms with filling traps completely were applied to the MOS structures (A-B key in B position) to measure ARS transients. The differential ARS, δU_{ac} was then monitored as a function of temperature and peaks with maxima of the temperature for which the emission rate is the same as the adjusted sample rate are observed in A-DLTS spectra. The A-DLTS experimental results were at temperatures varying between 373 and 77 K, samples were cooled in nitrogen cryostat. The $U_{ac}^0 - U_g$ curves were measured using the programmable voltage source, type HAMEG-HM 8131-2, providing both the linear increase (decrease) of the gate bias and the variation of increasing (decreasing) rate. The

Document downloaded by @DAEL, 2026-05-09 14:57:29 - personal use only

Table I. Summary of investigated Si MOS structures and their characteristics. *: Original identification: NA-7POA, NB-3POA, PA-P2.

Sample*	Thickness (nm)	Si type	Treatment
NA	3.5	n	POA at 250 ^{0}C in N_2 for 1 h
NB	9.2	n	POA at 250 ^{0}C in N_2 for 1 h
PA	2.4	p	No treatment

$U_{ac}^0 - U_g$ characteristics were measured at room temperatures ($\sim$ 300 K) and determined interface states distributions were also compared with A-DLTS results.

As it was already mentioned the sensitivity of the used acoustic spectrometer to determine the density of interface states depends on several parameters given by both experimental arrangement and following calculation procedure. The calculated sensitivity limit for our experimental arrangement is 5.0×10^{10} eV^{-1}cm^{-2}. However, in the case of measured MOS structures, especially those with thinner oxide layers, the stability of the measured acoustoelectric signal allowed to determine the density of interface states only with the sensitivity better than 1.0×10^{11} eV^{-1}cm^{-2}.

To know the electrical characteristics, the current-voltage ($I-V$) and capacitance-voltage ($C-V$) characteristics were recorded with HP 4192A impedance analyzer and/or FLUKE PM 6306 programable automatic RLC meter.

The acoustoelectric investigation of interface states using introduced theoretical principles was applied to the Si MOS structures with very thin oxides prepared on both n- and p-type Si substrates growing by nitric acid (HNO_3) oxidation method of Si (NAOS), which can be performed at relatively low temperatures ($\sim$ 120^0C) [17, 55].

N-Si MOS structures (NA, NB) were fabricated from phosphorus-doped Si (100) wafers with $\sim$ 10 Ωcm resistivity. After cleaning the wafers using RCA method and etching with dilute hydrofluoric acid, they were immersed in HNO_3 aqueous solutions of concentrations, 62 % and 58 %, respectively at temperature $\sim$ 120^0C for different reaction times to prepare different oxide thickness (NA-4 h, NB-10 h). P-Si MOS structure (PA) were fabricated on boron-doped p-type Si(100) wafers with $10 - 15$ Ωcm resistivity. After RCA cleaning of the Si wafers and the removal of a native oxide layer, a thin oxide layer was formed by immersing the Si wafers in 62 % HNO_3 aqueous solutions at 120^0C for 2 h. The aluminum (Al) dots of 0.15 and 0.30 mm diameter were formed on all parts of prepared wafers, resulting in <Al/SiO_2/Si> MOS diodes. The thickness of the SiO_2 layer was estimated from XPS and/or ellipsometry measurements.

The investigated set of Si MOS structures including the type of Si, the oxide thickness and some other parameters are summarized in Table I. The presented choice of MOS structures was made to represent the results obtained on various types of structures including n- and p-type Si substrates as well as various oxide thickness.

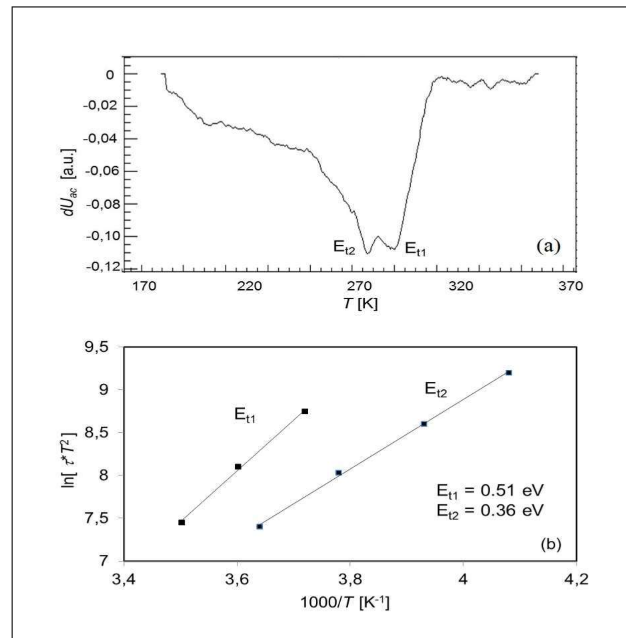

Figure 9. A-DLTS spectrum of Si MOS structure NA (a) and corresponding Arrhenius plots (b).

5. Results and discussion

The presented parameters and distribution of interface states of representative set of Si MOS structures were obtained using the measured A-DLTS spectra, $U_{ac}^0 - U_g$ characteristics and theoretical principles described before. Figure 9a presents A-DLTS spectrum obtained on n-type Si MOS structure (NA) with 3.5 nm thick oxide and Figure 9b calculated Arrhenius plots including obtained energies. The illustrated A-DLTS spectrum that was observed using pulse voltage ΔU_g = 2.5 V (U_g = -2.0 V) contains one evident double peak with maxima at 270 K and 300 K, respectively with some lateral structure at lower temperatures corresponding to lower energies. Figure 10a shows both measured and fitted (ideal) $U_{ac}^0 - U_g$ characteristics for the same structure. For simplification and better possibility to compare individual results, there is on x-axis indicated the difference $U_g - U_{fb}$, so that zero voltage corresponds to the flatband where the ARS reaches its minimum. The measured flatband was -0.65 V. Comparing the real and ideal characteristics, several detected humps at measured characteristic imply the presence of interface states. Fitted characteristic was calculated using following measured parameters related to the investigated structure, $N_D = 3.7 \times 10^{21}\ m^{-3}$; $C_{ox} = 9.87 \times 10^{-3}\ F/m^2$ and parameter extracted through the fitting process p_0 = 1.8×10^{11} Pa. Elastic moduli $K_s = 5.36 \times 10^{10}$ Pa and $K_i = 7.3 \times 10^{10}$ Pa for Si and SiO_2, respectively were used for all investigated structures. The distribution of interface states with respect to the energy levels across the bandgap of silicon, shown in Figure 10b, was then calculated by using measured and fitted (ideal) $U_{ac}^0 - U_g$ characteristics (Figure 10a). Comparing the A-DLTS results with the dis-

Document downloaded by @DAEL, 2026-05-09 14:57:29 - personal use only

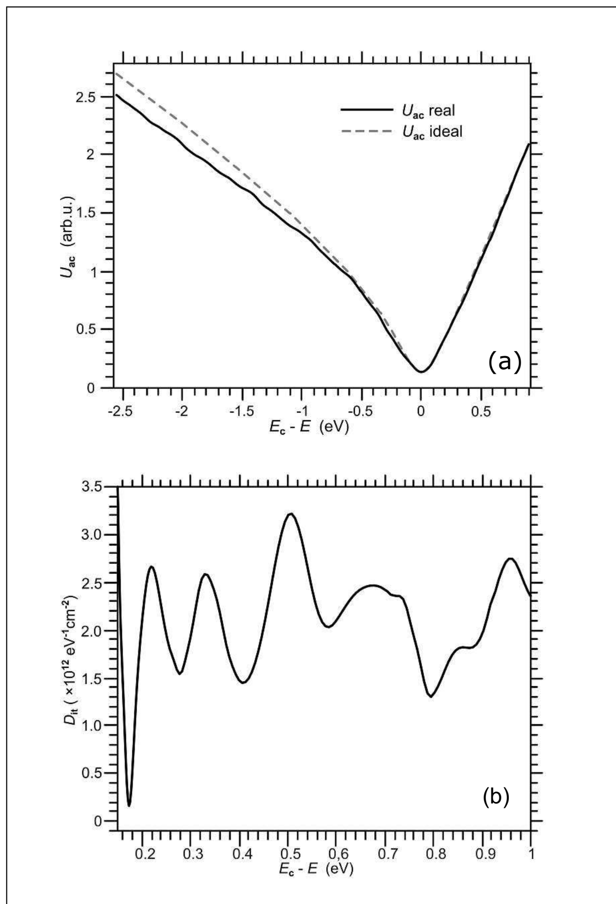

Figure 10. Measured and ideal $U_{ac}^0 - U_g$ curves (a) and calculated distributions of interface state density (b) for NA structure (d = 3.5 nm).

tribution of interface state, we can find quite good agreement in the position of energies.

The A-DLTS spectrum of another MOS structure prepared on n-type Si but with oxide thicknesses 9.2 nm (NB) and calculated Arrhenius plots are shown in Figure 11. The illustrated A-DLTS spectrum in this case at pulse voltage $\Delta U_g = 2.0$ V (U_g = -2.5 V) contains one broad triadic peak with maxima at 190, 230 and 250 K, corresponding to three different energies. The $U_{ac}^0 - U_g$ characteristics of the same structure and corresponding determined distributions of interfaced states are illustrated in Figure 12. Fitted characteristic was calculated using the following measured parameters related to the investigated structure, $C_{ox} = 3.84 \times 10^{-3}$ F/m^2, $U_{fb} = -1.45$ V and parameters extracted through the fitting process $p_0 = 1.95 \times 10^{11}$ Pa, $U_c = 0.2$ V.

The donor concentrations in both n-type Si wafers were the same. We can see on the real characteristics the similar process as in the case of previous structure, but with different region (beginning) of tunneling process which, in the case of thicker oxide layer, begins at higher reverse voltage that coincides with our assumption.

It should be noted that obtained results coincide very well with results obtained from the Acoustic-DLTS spectra which indicated interface states about, 0.63, 0.49 and

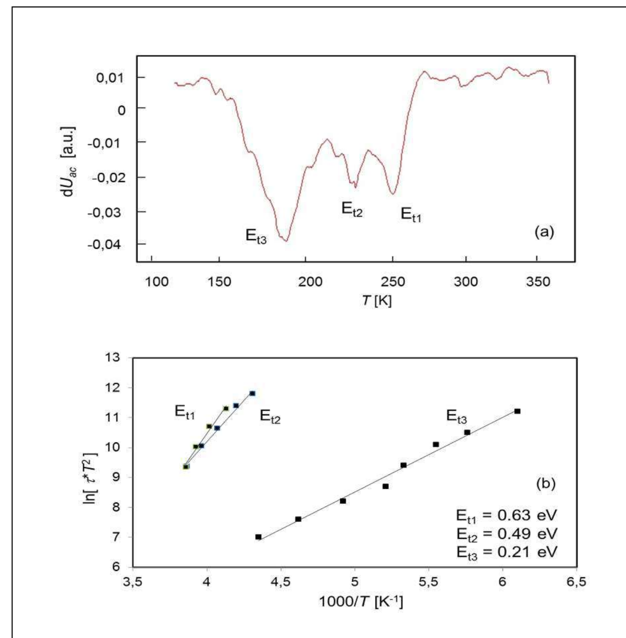

Figure 11. A-DLTS spectrum of Si MOS structure NB (a) and corresponding Arrhenius plots (b).

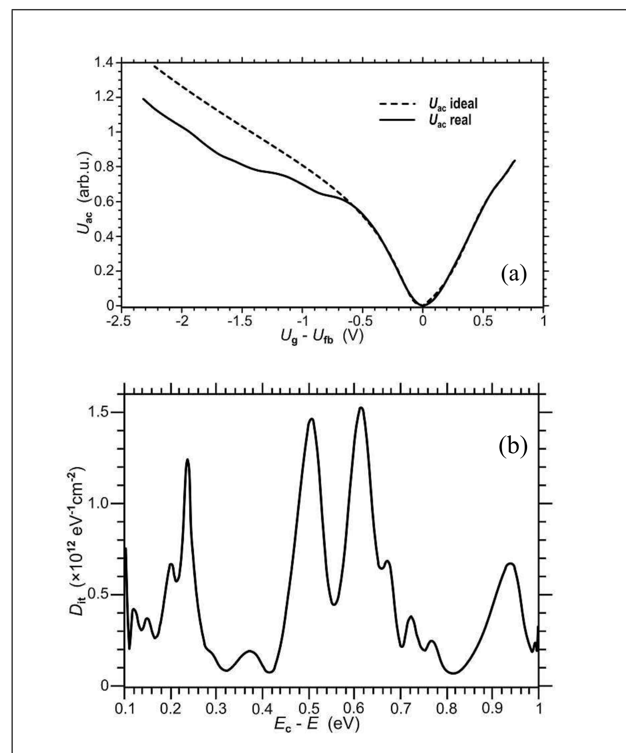

Figure 12. Measured and ideal $U_{ac}^0 - U_g$ curves (a) and calculated distributions of interface state density (b) for NB structure (d = 9.2 nm).

0.21 eV below the conduction band. Interface states with the energy near the midgap were observed for SiO_2/Si interfaces with very thin oxide also by means of XPS under bias. They are attributed to isolated Si dangling bonds, with which no atoms in the oxide layer interact. Interface states above the valence band and below conduction band

Document downloaded by @DAEL, 2026-05-09 14:57:29 - personal use only

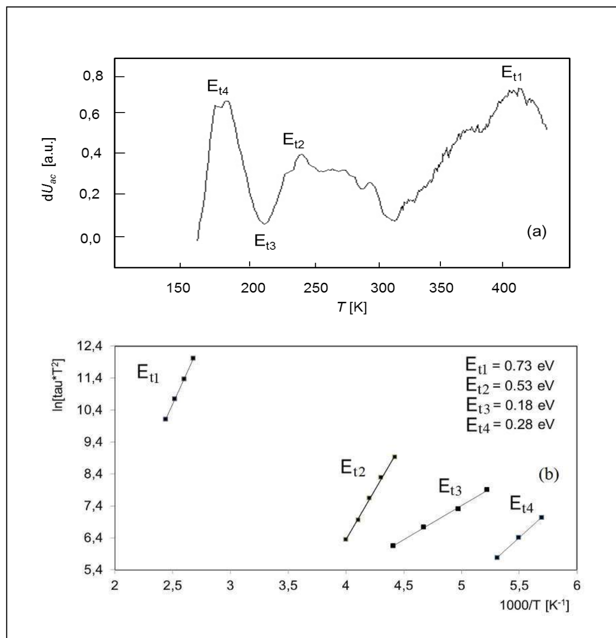

Figure 13. A-DLTS spectrum of Si MOS structure PA including corresponding Arrhenius plots incide (a) and distribution of interface state density calculated using measured and ideal $U_{ac}^{0} - U_{g}$ curves (b).

were attributed to Si dangling bonds interacting weakly with an oxygen or Si atom in the oxide layer [41].

Figure 13a shows the A-DLTS spectrum of p-Si MOS structure (PA) and Figure 13b corresponding Arrhenius plots and determined energies. The presented A-DLTS spectrum observed using the pulse voltage $\Delta U_g = -2.0\,\text{V}$ ($U_g = 0.5\,\text{V}$) shows three positive peaks with maxima at approximately 180, 240 and 400 K and one negative peak with maximum at 200 K, corresponding to different types of interface states a savoir to the donor type. Interface states distribution of the same MOS structure (Figure 14b) was calculated using measured and ideal curves of the ARS dependence on the gate voltage illustrated in Figure 14a. Fitted characteristic was calculated using following measured parameters related to the investigated structure, $NA = 4.0 \times 10^{22}$ m^{-3}, $C_{ox} = 3.45 \times 10^{-3}$ F/m^2, $U_{fb} = -0.95\,\text{V}$ and parameter extracted through the fitting process $p_0 = 4.3 \times 10^{10}$ Pa.

A-DLTS spectra of investigated sample correspond to the interface states of acceptor type with the activation energies 0.28, 0.53 and 0.73 eV above the valence band edge and donor type with the energy 0.18 eV under the conduction band. The observed energies coincide with the density of interface state distribution determined from $U_{ac} - U_g$ measurements. The interface states with an activation energy $\sim$ 0.2 eV should correspond to Si dangling bonds interacting weakly with oxygen or Si atoms having unpaired electron [39, 41]. The decrease of the density of interface state distribution after the thermal treatment can be attributed to the fact that the thermal treatment eliminates some suboxide species, which is a reason also for the decrease of the leakage current density [55].

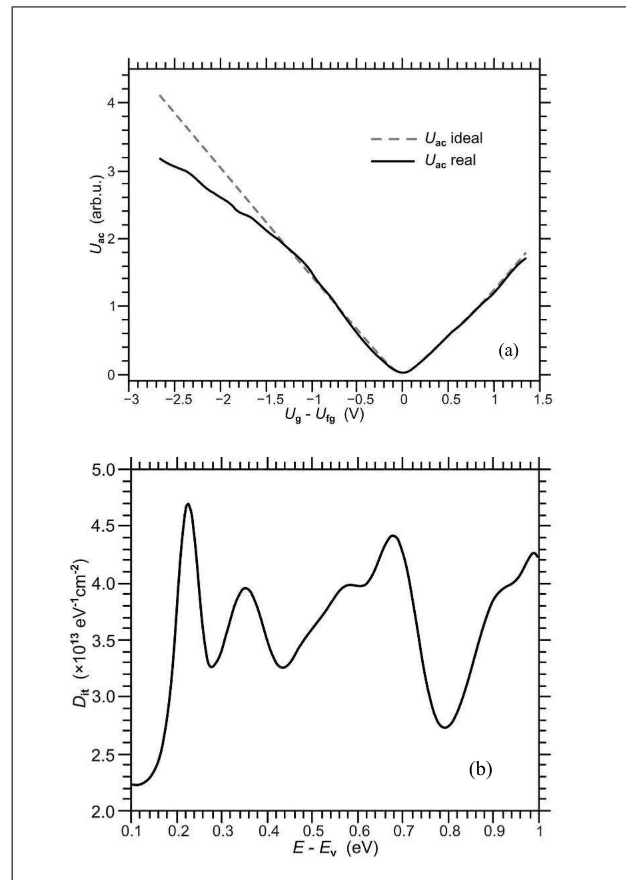

Figure 14. Measured and ideal $U_{ac}^{0} - U_{g}$ curves (a) and calculated distributions of interface state density (b) for PA structure (d = 2.4 nm).

We would like to note that some difference of presented results comparing with our previous results are caused by both the improvement of the acoustic spectrometer and the innovated procedure of the A-DLTS spectra analysis. However, these results are not in the discrepancy with previous ones, they only amplify them.

6. Conclusion

The investigation of interface states in MOS structures with very thin oxides by complete acoustic spectroscopy techniques utilizing the acoustoelectric response signal (ARS) produced by MOS interfaces when a longitudinal acoustic wave propagates through the structure namely as a function of both time after applied injection pulse (A-DLTS spectra) and the gate voltage ($U_{ac} - U_g$ characteristics) is presented as an effective tool for the characterization of interface states. Comparison of the measured and fitting (ideal) $U_{ac} - U_g$ characteristics allow to determine the interface states distribution and together with A-DLTS, it provides both complete acoustic investigation of MOS structures and also information comparable with $C - U_g$ and $G - U_g$ measurements. The presented technique used for interface states investigation induced also some advantages compared with other techniques: the ARS is pro-

Document downloaded by @DAEL, 2026-05-09 14:57:29 - personal use only

duced directly by the interface containing the space charge so that any changes in its distribution are immediately reflected by the ARS; the strong acousto-lattice interaction allows to discover some new interface states; the quality of the ohmic contacts should not play so important role as in electrical techniques.

The investigation of several kinds of MOS structures formed by various methods verified the presented method. The parameters and distributions of interface states were determined for MOS structures with very thin oxides prepared on both n- and p-type silicon wafers. The position of interface state energies obtained by A-DLTS coincides very well not only with results determined from $U_{ac} - U_g$ characteristics but also with results obtained by different techniques.

Acknowledgements

The authors would like to thank Prof. Hikaru Kobayashi from Institute of Scientific and Industrial Research, Osaka University, CREST, Japan Scienceand Technology Organization, 8-1 Mihogaoka, Ibaraki, Osaka 567-0047, Japan for samples providing and Mr. F. Černobila for technical assistance. This work was financially supported by the R&D operational program Centrum of excellence of power electronics systems and materials for their components, No. ITMS 26220120003 funded by European Community and project ITMS: 26210120021, co-funded from EU sources and European Regional Development Fund.

References

[1] A. R. Huton, J. H. McFee, D. L. White: Ultrasonic Amplification in CdS. Physical Review Letters **7** (1961) 237.

[2] H. N. Spector: Effect of an External Electric Field on the Velocity of Sound in Semiconductors and Semimetals. Physical Review **134** (1964) A507.

[3] J. H. McFee: Phycical Acoustics IV Part A.1, Ed. W. Mason, Academic Press, London/New York, 1966.

[4] S. Y. Mensah, F. K. A. Allotey, N. G. Mensah: Nonlinear acoustoelectric effect in a semiconductor superlattice. Journal of Physics: Condensed Matter **12** (2000) 5225.

[5] S. Y. Mensah, N. G. Mensah, V. W. Elloh, G. K. Banini, F. Sam, F. K. A. Allotey: Propagation of ultrasonic waves in bulk gallium nitride (GaN) semiconductor in the presence of high-frequency electric field. Physica E **28** (2005) 500-506.

[6] M. Tabib-Azar, P. Das: Surface acoustic wave-superlattice interactiom in separate-medium structure. Superlattices and Microstructures **4**(4/5) (1988) 643-651.

[7] I. V. Ostrovskij, O. Ya. Olikh: Characterization of interface deep levels in As vapor grown EPI-GaAs. Solid State Communications **107**(7) (1998) 341-343.

[8] A. Abbate, K. J. Man, I. V. Ostrovskij, P. Das: Acoustoelectric deep-level transient spectroscopy in semiconductors. Solid State Electronics **36** (1993) 697-703.

[9] A. O. Govorov, A. V. Kalameitsev, M. Rotter, A. Wixforth, J. P. Kothaus, K. H. Hoffmann, N. Botkin: Nonlinear acoustoelectric transport in a two-dimensional electron system. Physical Review B **62** (2000) 2659.

[10] N. V. Nghia, T. T. T. Huong, N. Q. Bau: The nonlinear acoustoelectric effect in a cylindrical quantum wire with an infinite potential. Proceedings National Conference on Theorreticl Physicis **35** (2010) 183.

[11] C. L. Foden, V. I. Talyanskii, G. J. Milburn, M. L. Leadbeater, M. Pepper: High-frequency acousto-electric single-photon source. Physical Review A **62** (2000) 11803.

[12] J. Cunningham, M. Pepper, V. I. Talyanskii, D. A. Ritchie: Acoustoelectric current in submicron-separated quantum wires. Applied Physics Letters **86** (2005) 152105.

[13] E. S. Young, A. V. Akimov, M. Henini, L. Eaves, A. J. Kent: Subterahertz Acoustical Pumping of Electronic Charge in a Resonant Tunneling Device. Physical Review Letters **108**(22) (2012) 226601.

[14] S. Middleman, A. K. Hochberg: Process Engineering Analysis in Semiconductor Device Fabrication, McGraw/Hill, Inc. 1993.

[15] E. M. Nicollian, J. R. Brews: MOS (Metal Oxide Semiconductor) Physics and Technology, NewYork, Wiley, 1982.

[16] B. H. Kim, J. H. Ahn, B. T. Ahn: Finding interstitial oxygen in an Si substrate during low-temperature plasma oxidation. Applied Physics Letters **82**(16) (2003) 2682.

[17] H. Kobayashi, T. Yuasa, Y. Nakato, K. Yoneda, Y. Todokoro: Low temperature catalytic formation of Si-based metal-oxide-semiconductor structure. Journal of Applied Physics **80**(7) (1996) 4124.

[18] A. Asuha, T. Kobayashi, O. Maida, M. Inoue, M. Takahashi, Y. Todokoro, H. Kobayashi: Ultrathin silicon dioxide layers with a low leakage current density formed by chemical oxidation of Si. Applied Physics Letters **81**(18) (2002) 3410.

[19] H. Kobayashi, A. Asuha, O. Maido, M. Takahashi, M. Iwasa: Nitric acid oxidation of Si to form ultrathin silicon dioxide layers with a low leakage current density. Journal of Applied Physics **94**(11) (2003) 7328.

[20] M. L. Green, E. P. Gusev, R. Degraeve, E. L. Carfunkel: Ultrathin (<4 nm) SiO2SiO_2 and Si-O-N gate dielectric layers for silicon microelectronics: Understanding the processing, structure, and physical and electrical limits. Journal of Applied Physics **90**(5) (2001) 2057.

[21] H. Castán, S. Dueňas, H. Garcia, A. Gómez, L. Bailón, M. Toledano-Luque, A. del Prado, I. Mártil, G. González-Díaz: Effect of interlayer trapping and detrapping on the determination of interface state densities on high-k dielectric stacks. Journal of Applied Physics **107**(11) (2010) 114104.

[22] L. M. Terman: An investigation of surface states at a silicon/silicon oxide interface employing metal-oxide-silicon diodes. Solid State Electronics **5**(5) (1962) 285-299.

[23] E. H. Nicollian, A. Goetzberger, C. N. Berglund: Avalanche injection currents and charging phenomena in thermal SiO_2. Applied Physics Letters **15**(6) (1969) 174.

[24] D. R. Young, E. A. Irene, D. J. DiMaria, R. F. Keersmaecker, H. Z. Massoud: Electron trapping in SiO_2 at 295 and 77 K. Journal of Applied Physics **50** (1979) 6366.

[25] W. L. Tseng: A new charge pumping method of measuring Si/SiO_2 interface states. Journal of Applied Physics **62** (1987) 591.

[26] K. Pater: Surface photovoltage measurement in MOS structures,. Applied Physics A **44** (1987) 191-194.

[27] K. K. Hung, Y. C. Cheng: Characterization of Si/SiO_2 interface traps in p-metal-oxide-semiconductor structures with thin oxides by conductance technique. Journal of Applied Physics **62** (1987) 4204.

Document downloaded by @DAEL, 2026-05-09 14:57:29 - personal use only

[28] D. V. Lang: Deep-level transient spectroscopy: A new method to characterize traps in semiconductors. Journal of Applied Physics **45** (1974) 3023.

[29] K. Yamasaki, M. Yoshida, T. Sugano: Deep Level Transient Spectroscopy of Bulk Traps and Interface States in Si MOS Diodes. Japanese Journal of Applied Physics **18** (1979) 113-122.

[30] K. I. Kirov, K. B. Radev: A simple charge-based DLTS technique. physica status solidi (a) **63** (1981) 711-716.

[31] V. I. Turchanikov, V. S. Lysenko, V. A. Gusev: Isothermal DLTS method using sampling time scanning. physica status solidi (a) **95** (1986) 283-289.

[32] M. Schulz, N. M. Johnson: Transient capacitance measurements of hole emission from interface states in MOS structures. Applied Physics Letters **31** (1977) 622.

[33] W. A. Doolittle, A. Rohatgi: A novel computer based pseudo-logarithmic capacitance/conductance DLTS system specifically designed for transient analysis. Review of Scientific Instruments **63** (1992) 5733.

[34] C. R. Crowell, S. Alipanahi: Transient distortion and nth order filtering in deep level transient spectroscopy (D^nLTS). Solid-State Electronic **24** (1981) 25-36.

[35] C. W. Wang, C. H. Wu, B. L. Boone: A new technique to decompose closely spaced interface and bulk trap states using temperature dependent pulse-width deep level transient spectroscopy method: An application to PT/CdS photodetector. Journal of Applied Physics **73** (1993) 760.

[36] L. Dobaczewski, P. Kaczor, I. D. Hawkins, A. R. Peaker: Laplace transform deep-level transient s ectroscopic studies of defects in semiconductors. Journal of Applied Physics **76**(1) (1994) 194.

[37] K. Dmowski: Side data analysis of deep level transient spectroscopy spectra for a multipoint correlation method with binomial weighting coefficients. Solid State Electronics **38** (1995) 1051-1057.

[38] P. Masson, J. L. Autran, M. Houssa, X. Garros, Ch. Leroux: Frequency characterization and modeling of interface traps in gate dielectric stack from a capacitance point-of-view. Applied of Physics Letters **81** (2002) 3392.

[39] N. Inoue, D. J. Lichtenwalter, J. S. Jur, A. I. Kingon: Analysis of Interface States in LaSixOy Metal-Insulator-Semiconductor Structures. Japanese Journal of Applied Physics **46** (2007) 6480.

[40] I. V. Antonova, J. Stano, O. V. Naumova, V. P. Popov, V.A. Skuratov: DLTS study of bonded interface in silicon-on-insulator structures annealed in hydrogen atmosphere. Microelectronics Engineering **66** (2003) 547-552.

[41] H. Kobayashi, A. Asada, T. Kubota, Y. Yamashita, K. Yoneda, Y. Todokoro: Studies on interface states at ultrathin interfaces by means of x-ray photoelectron spectroscopy under biases and their passivation by cyanide treatment. Journal of Applied Physics **83**(4) (1998) 2098.

[42] A. Abate, P. Das: Ultrasonic Symposium 1990, Proceedings, IEEE (1990) 459.

[43] I. V. Ostrovskij, O. Ya. Olikh: Charakterization of interface deep levels in As vapor grown EPI-GaAs. Solid State Communications **107**(7) (1998) 341-343.

[44] A. Abbate, K. J. Man, I. V. Ostrovskij, P. Das: Acoustoelectric deep-level transient spectroscopy in semiconductors. Solid State Electronics **36**(5) (1993) 697-703.

[45] M. M. Abedin, P. Das: A study of deep levels of semi-insulating InP: Fe using nondestructive transverse acoustoelectric voltage spectroscopy. Semiconductor Science and Technology **3**(6) (1988) 623.

[46] P. Bury, I. Jamnický, V. W. Rampton: Acoustic spectroscopy of deep centres in GaAs/AlGaAs heterostructures. Physica B: Condensed Matter **263-264** (1999) 94-97.

[47] P. Bury, T. Matsumoto, Š. Hardoň, I. Bellan, M. Janík, H. Kobayashi: Investigation of interface states in Si/NAOS-SiO_2/HfO_2 sturctures using complete acoustic spectroscopy. Communications **16**(1) (2014) 3-9.

[48] P. Bury, J. Ďurček, K. Sakalauskas: On the piezoactivity of si MOS structures. physica status solidi (a) **95** (1986) K207-K209.

[49] P. Bury, I. Jamnický, J. Ďurček: Acoustic Deep-Level Transient Spectroscopy of MIS Structures. physica status solidi (a) **126**(1) (1991) 151-161.

[50] P. Bury, I. Jamnický: PC operated acoustic transient spectroscopy of deep levels in MIS structures. acta phys. slovaca **46**(6) (1996) 693-700.

[51] P. Bury, T. Matsumoto, I. Bellan, M. Janík, H. Kobayash: Acoustic spectroscopy and electrical characterization of Si/NAOS-SiO_2/HfO_2 structures. Applied Surface Sciences **269** (2013) 50-54.

[52] P. Bury, I. Bellan, H. Kobayashi, M. Takahashi, T. Matsumoto: Investigation of interface states distribution in metal-oxide-semiconductor structures with very thin oxides by acoustic spectroscopy. Journal of Applied Physics **116**(14) (2014) 144302.

[53] I. Jamnický, P. Bury: Acoustic version of Lang's DLTS for MIS structure investigation. physica status solidi (a) **139** (1993) K35.

[54] P. Hockicko, P. Bury, P. Sidor, H. Kobayashi, M. Takahashi, T. Yanase: Analysis of A-DLTS spectra of MOS structures with thin NAOS SiO_2 layers. Central European Journal of Physics **9**(1) (2011) 242.

[55] P. Bury, H. Kobayashi, M. Takahashi, K. Immamura, P. Sidor, F. Černobila:Acoustic spectroscopy and electrical characterization of SiO_2/Si structures with ultrathin SiO_2 layers formed by nitric acid oxidation. Central European Journal of Physics **7**(2) (2009) 237.

[56] J. Racko, P. Valent, P. Benko, D. Donoval, L Harmatha, P. Pinteš, J. Breza: Unified tunnelling-diffusion theory for Schottky and very thin MOS structures. Solid State Electronics **52** (2008) 1755-1765.

[57] S. M. Sze: Physics of Semiconductor Devices. Wiley, New York, 1981.

Document downloaded by @DAEL, 2026-05-09 14:57:29 - personal use only